HAL
open science

Why is Mechanical Fatigue Different from Toughness in Elastomers? The Role of Damage by Polymer Chain Scission

Gabriel E Sanoja, Xavier P Morelle, Jean Comtet, C. Joshua Joshua Yeh, Matteo Ciccotti, Costantino Creton

To cite this version:

Gabriel E Sanoja, Xavier P Morelle, Jean Comtet, C. Joshua Joshua Yeh, Matteo Ciccotti, et al.. Why is Mechanical Fatigue Different from Toughness in Elastomers? The Role of Damage by Polymer Chain Scission. 2021. hal-03871381v1

HAL Id: hal-03871381

https://espci.hal.science/hal-03871381v1

Preprint submitted on 16 Sep 2021 (v1), last revised 25 Nov 2022 (v2)

HAL is a multi-disciplinary open access archive for the deposit and dissemination of scientific research documents, whether they are published or not. The documents may come from teaching and research institutions in France or abroad, or from public or private research centers.

L'archive ouverte pluridisciplinaire **HAL**, est destinée au dépôt et à la diffusion de documents scientifiques de niveau recherche, publiés ou non, émanant des établissements d'enseignement et de recherche français ou étrangers, des laboratoires publics ou privés.

FRONT MATTER

Title

Why is Mechanical Fatigue different from Toughness in Elastomers? The Role of Damage by Polymer Chain Scission

Authors

Gabriel E. Sanoja[1,2,*], Xavier P. Morelle[1,†], Jean Comtet[1], C. Joshua Yeh[1,‡], Matteo Ciccotti[1], and Costantino Creton[1,3]

Affiliations

[1]Sciences et Ingénierie de la Matière Molle, ESPCI Paris, Université PSL, Sorbonne Université, CNRS UMR 7615, 75005, Paris, France.
[2]McKetta Department of Chemical Engineering, The University of Texas at Austin, Austin, Texas, 78712, United States
[3]Global Station for Soft Matter, Global Institution for Collaborative Research and Education, Hokkaido University, 001-0021, Sapporo, Japan.
[†]Present address: Ingénierie des Matériaux Polymères, Université Claude Bernard Lyon 1, INSA de Lyon, Université Jean Monnet de St Etienne, CNRS UMR 5233, 69622, Villeurbanne, France
[‡]Present address: 3M Research Center, Saint Paul, Minnesota, 55144, United States
*Corresponding author. Email: gabriel.sanoja@espci.psl.eu

Abstract

Although elastomers often experience 10-100 million cycles prior to failure, there is currently a limited understanding of their resistance to fatigue crack propagation. We use soft and tough double-network elastomers tagged with mechanofluorescent probes to understand the role of damage by sacrificial bond scission on their mechanical durability and fracture toughness. Damage accumulation and localization ahead of the crack tip depend on the areal density of sacrificial bonds, as well as on the applied load (*i.e.*, cyclic or monotonic). This information serves to engineer fatigue resistant elastomers, understand fracture mechanisms, and reduce the environmental footprint of the polymer industry.

Teaser

Quantification of damage reveals that tough elastomers that resist fracture at high loads are not optimum for sustaining many cycles at low loads.

MAIN TEXT

Introduction

Elastomers are ubiquitous in engineering applications that require large reversible deformations such as tyres, belts, dampers, and seals (*1*). Although toughness remains an important design consideration to prevent catastrophic failure at high loads, mechanical lifetime is often controlled by the progressive growth of an inherent flaw over numerous cycles of low load. This mechanical degradation is evaluated with durability tests based on *fatigue crack propagation*, where the crack growth rate of a pre-cracked specimen is monitored over a range of cyclic deformations (or energy release rates) (*2*, *3*). Typically, elastomers suffer from fatigue crack propagation at low cyclic loads, and exhibit cyclic fatigue thresholds $\mathcal{G}_0 \sim$ 0.05-0.1 kJ.m^{-2} (at which the crack is effectively stopped) significantly below the fracture toughness $\mathcal{G}_c \sim$ 1-100 kJ.m^{-2} (as measured by

crack propagation under monotonic loading) (*4*, *5*). A fundamental understanding of this fracture behavior would serve to mitigate over-engineering, extend lifetime, and facilitate the transition towards a more sustainable elastomer economy.

Fatigue crack propagation has been previously investigated in elastomers (*3*, *6–8*), and more recently in hydrogels (*9–12*). A comparison of the fracture behavior of these materials under monotonic and cyclic loading illustrates some vexing features of fatigue crack propagation. Under monotonic loading, pre-cracked specimens of hydrogels based on ionically crosslinked alginate interpenetrated with covalently crosslinked polyacrylamide exhibit a fracture toughness $\mathcal{G}_c$ ~10 kJ.m^{-2} similar to that of filled elastomers (*13*). However, under cyclic loading these hydrogels have a crack growth rate *dc/dN* ~ 100 nm.cycle^{-1} significantly higher than that of filled elastomers *dc/dN* ~ 1 nm.cycle^{-1} at the same applied energy release rate $\mathcal{G}$ ~ 0.1 kJ.m^{-2} (*7*, *10*). These observations indicate that filled elastomers have a longer mechanical lifetime than hydrogels, but also that the mechanisms responsible for reinforcement change when transitioning from monotonic to cyclic loading. This is the reason why energy dissipation by irreversible damage during the first cycle of deformation (*i.e.*, so-called Mullins effect) is not necessarily correlated with fatigue resistance (*11*, *12*). As the subsequent cycles are usually at high frequency and low load, it is the evolution of the crack tip with sustained opening and closing that is presumably key for fatigue crack propagation.

Here, we use soft and tough double-network (DN) elastomers as model materials to investigate fatigue crack propagation. These are composed of a pre-stretched, stiff, and continuous *filler* network embedded in a highly extensible, soft, and incompressible *matrix* network. Even though their elastic properties are mainly controlled by the filler network, as in conventional filled elastomers, their fracture toughness primarily results from energy dissipation by sacrificial bond scission during stress transfer to the matrix network (*14*, *15*). This toughening mechanism was recently demonstrated by tagging the filler network with mechanoluminescent damage-activated probes (*i.e.*, mechanophores), monotonically loading a pre-cracked specimen, and visualizing sacrificial bond scission ahead of the crack tip in a time-resolved manner (*16*). However, under cyclic loading a similar pre-cracked specimen suffers negligible scission of sacrificial bonds per cycle, making visualization of *cumulative damage by sacrificial bond scission* more valuable to understand fatigue crack propagation. Thus, we tagged the filler network of DN elastomers with mechanofluorescent probes based on π-extended anthracene-maleimide adducts. Upon polymer chain elongation until failure, these probes undergo a force-induced cycloreversion reaction that results in π-extended anthracene moieties (*i.e.*, fluorophores) of high quantum yield, stability to photobleaching (*17*, *18*), and ideal for visualizing and quantifying damage by sacrificial bond scission near the crack surface of fractured specimens (*19*). This combination of network design and damage quantification is what ultimately provides novel insights on the difference between mechanical durability and fracture toughness in elastomers.

We synthesized two DN elastomers through sequential free radical polymerization of ethyl acrylate (EA). Detailed synthetic conditions, compositions, and mechanical properties are provided in the Supporting Information (SI, Fig. S1, Table S1-S3) but their primary difference lies in the crosslinking density of the filler network, which is 0.2 mol% for $EA_{0.2}EA$ and 0.5 mol% for $EA_{0.5}EA$. Thus, $EA_{0.2}EA$ is tougher and more extensible than $EA_{0.5}EA$ (see onset of strain hardening and strain at break in Fig. 1), even if both elastomers have the same monomer composition, pre-stretch of the filler network, Young's modulus (Table 1, inset of Fig. 1), and negligible mechanical hysteresis under step-cyclic loading until fracture (Fig. S3). This elastic behavior (*i.e.*, lack of mechanical hysteresis) suggests that sacrificial bond scission is inconsequential for energy dissipation during crack propagation, an observation that is misleading

because sacrificial bond scission is actually localized in a large strain region ahead of the crack tip referred to as *damage zone* (*16*).

Differences in mechanical properties between the two DN elastomers are subtle but important for rationally engineering fatigue resistant elastomers. As outlined by Suo and co-workers in their seminal investigations on hydrogels, energy dissipation by sacrificial bond scission leads to toughening in monotonic loading, but accumulation of these scission events ahead of the crack tip could favor crack growth and decrease fatigue resistance (*11*, *12*). Given that $EA_{0.2}EA$ and $EA_{0.5}EA$ exhibit near-perfect elasticity until failure, we deemed them good model materials to (i) investigate the role of crosslinking density of the filler network on fatigue crack propagation, and (ii) build a multi-scale picture of fracture under cyclic and monotonic loading using mechanofluorescent probes to reconstruct 3-D maps of cumulative damage by sacrificial bond scission.

Trade-off between Durability and Toughness in DN Elastomers

We evaluated the fatigue crack propagation of the two DN elastomers with durability tests similar to those pioneered for vulcanized elastomers (*20*) and tough hydrogels (*12*). Pre-cracked pure-shear specimens were subjected to cyclic loading at a frequency of 10 Hz and an applied energy release rate $\mathcal{G}$, and the evolution of the crack length c monitored with the applied number of cycles N (Fig. 2A). These durability tests on specimens of pure-shear geometry lead to an applied energy release rate $\mathcal{G}$ independent of crack length c (*20*, *21*), enabling optimum use of mechanofluorescent probes by applying a range of energy release rates $\mathcal{G}$ to the same tagged specimen in a successive and stepwise fashion (see detailed estimates of $\mathcal{G}$ from λ in the SI, pure-shear loading curves in Fig. S4, and loading conditions in Table S5). Results are presented in Fig. 2B (and Fig. S5A) and indicate that the crack length c grows discontinuously (*i.e.*, non-steadily) with the applied number of cycles N, meaning that there is a distribution of crack growth rates dc/dN for each applied $\mathcal{G}$ (see example for $\lambda = 1.47$ in inset of Fig. 2B). Average crack growth rates dc/dN and 95% confidence intervals are summarized in Fig. 2C and reveal a power-law (*i.e.*, Paris' law) behavior $dc/dN \sim \mathcal{G}^{3.4}$ for DN elastomers like that of natural rubber (*4*), SBR (*5*), and DN hydrogels (*11*). Fig. 2C also illustrates that two crack growth regimes, referred to as *fast* and *slow* due to their distinct dc/dN, coexist near the onset of catastrophic failure (see filled and empty squares in Fig. 2C, and videos of fatigue fracture tests in Movies S1-S2). These are observed at $\mathcal{G} \approx \mathcal{G}_c$ for $EA_{0.5}EA$, but at $\mathcal{G} \ll \mathcal{G}_c$ for $EA_{0.2}EA$ (compare dashed lines at $\mathcal{G}_c$ with empty squares at $\mathcal{G}$ at break in Fig. 2C), indicating that subtle changes in the crosslinking density of the filler network have major consequences in the fatigue crack propagation of DN elastomers. $EA_{0.5}EA$ is more fatigue resistant than $EA_{0.2}EA$ because it exhibits a lower crack growth rate dc/dN at the same applied energy release rate $\mathcal{G}$, but it is also more brittle because it undergoes catastrophic crack propagation under monotonic loading at a lower critical energy release rate $\mathcal{G}_c$. This trade-off between durability and toughness when stiffening the *filler* network is remarkable when compared to previous reports by Suo and coworkers on DN hydrogels with bulk energy dissipation, where stiffening the *matrix* network results in both a lower fatigue threshold and fracture toughness (*11*, *12*). Thus, both the filler and matrix networks play a role on fracture under monotonic and cyclic loading, but this is challenging to understand solely by bulk mechanical testing, particularly in DN elastomers without hysteresis under step-cyclic loading until failure.

Fig. 2C can also be used to estimate the cyclic fatigue threshold $\mathcal{G}_0$ from the energy release rate $\mathcal{G}$ at which the crack does not grow. Though the cyclic fatigue threshold $\mathcal{G}_0$ is theoretically well-defined, experimentally there is always a concern about the number of cycles used to detect crack

growth. Here, we had a spatial resolution of 250 μm.pixel^{-1} while monitoring the crack length *c*, meaning that the minimum crack growth rate *dc/dN* that we could measure over a basis of 400,000 cycles is of order 1 nm.cycle^{-1}. This threshold condition is more rigorous (and time consuming) than the 100 nm.cycle^{-1} used for tough hydrogels (*10*, *11*), but still one order of magnitude below the 0.1 nm.cycle^{-1} used for commercial metallic alloys (*22*). As $EA_{0.2}EA$ exhibits crack growth rates *dc/dN* ~ 10 nm.cycle^{-1} even at low $\mathcal{G}$ ~ 290 J.m^{-2}, we only determined the cyclic fatigue threshold $\mathcal{G}_0$ ~ 550 J.m^{-2} of $EA_{0.5}EA$. This $\mathcal{G}_0$ is similar to that of composite elastomers based on a hard elastomeric lattice embedded in a soft matrix (*8*), and remarkable when compared to that of conventional elastomers $\mathcal{G}_0$ ~ 50 J.m^{-2} (*23–25*) and single-network $EA_{0.5}$ (we did not measure $\mathcal{G}_0$ for single-network $EA_{0.5}$, but we expect it to be below its fracture toughness $\mathcal{G}_c$ ~ 150 J.m^{-2}). Thus, sacrificial bonds provide elastomers with both improved cyclic fatigue thresholds and fracture toughness. This reinforcement under both cyclic and monotonic loading is analogous to that reported by Suo and coworkers on tough hydrogels (*10*, *11*, *13*, *26*), and intrinsic to the DN architecture. However, the reinforcement mechanism is different. While energy dissipation by sacrificial bond scission is essential for toughening, its role on fatigue resistance remains unclear. A previous model on fatigue crack propagation in glassy polymers, where toughening results from damage by plastic flow (*i.e.*, crazing), suggests that formation of a crazed region ahead of the crack tip favors crack growth under cyclic loading (*27*). However, it is unclear whether this model also describes rubbery DN elastomers (T_g = -15 ^{o}C) that develop a damage zone prior to crack growth. To gain insights into the role of molecular damage on fatigue crack propagation, we reconstructed 3-D maps of damage by sacrificial bond scission in the fractured DN elastomers.

Visualization and Quantification of Damage by Sacrificial Bond Scission

Post-mortem fluorescent maps of the fracture surface enable visualization and quantification of damage accumulated ahead of the crack tip both before and during crack growth (see example of fluorescent image in Fig. 3B). Details of the methodology are provided in the SI and in a recent contribution from our group (*19*). The general idea is based on using the fluorescence of a 3-D slab to quantify the per-voxel fraction ϕ_{xyz} of π-extended anthracene moieties resulting from a force-induced cycloreversion reaction in the filler network (Fig. 3A). Given that the probability to break a polymer chain diverges near its limiting extensibility, we considered ϕ_{xyz} as representative of the fraction of bond scission events in the filler network (this hypothesis has been verified in previous work (*19*)). Averaging along the crack length *x* and specimen thickness *z* (see Fig. 3B) results in profiles of sacrificial bond scission as a function of the distance *y* away from the crack surface:

$$\varphi_y = \left(\frac{1}{wt}\right) \int_0^t \int_0^w \varphi_{xyz}\, dx\, dz \qquad \text{(Eq. 1)}$$

Where *w* is the width (1000 μm) and *t* the thickness (160 μm) of the 3-D fluorescent slab. Alternatively, integrating ϕ_{xyz} over a distance *L* along *y* yields spatial maps of *local damage per unit area of crack propagation* $\overline{\Sigma_{xz}}$:

$$\overline{\Sigma_{xz}} = 2\left(\frac{\nu_x}{\Sigma_0}\right) \int_0^L \varphi_{xyz}\, dy \qquad \text{(Eq. 2)}$$

Where ν_x and Σ_0 are the volumetric and areal density of elastic polymer chains determined from the modulus of the filler network (Table S2, S4). We set $L \approx 300$ μm to optimize the trade-off between optical vignetting and resolution of the damage zone near the crack surface. Noteworthy,

Eq. 1 and Eq. 2 are complementary and serve to define a dimensionless number representing the *overall damage per unit area of crack propagation* $\bar{\Sigma}$:

$$\bar{\Sigma} = \frac{\Sigma}{\Sigma_0} = 2\left(\frac{\nu_x}{\Sigma_0}\right)\int_0^L \varphi_y \, dy = \left(\frac{1}{wt}\right)\int_0^t \int_0^w \overline{\Sigma_{xz}} \, dx \, dz \quad \text{(Eq. 3)}$$

The physical meaning of $\bar{\Sigma}$ is based on the Lake and Thomas molecular theory of fracture of unfilled single-network elastomers (*23*), where the energy dissipated upon creation of an interface Γ_0 is that required to break a monolayer of stretched elastic polymer chains:

$$\Gamma_0 = N_x U_b \Sigma_0 \qquad \text{(Eq. 4)}$$

Where N_x is the number of monomers per elastic polymer chain, and U_b is the energy stored per C-C bond along the stretched polymer backbone (traditionally the energy of a C-C bond ≈ 350 kJ.mol^{-1}, but recently revised by Craig and coworkers to ≈ 60 kJ.mol^{-1} based on a probabilistic view of bond scission (*28*)). As such, $\bar{\Sigma}$ represents the excess number of broken layers in the filler network per unit area of crack growth, and is related to the energy dissipated by covalent bond scission upon fracture Γ_d:

$$\Gamma_d = \Gamma_0 \bar{\Sigma} = N_x U_b \Sigma_0 \bar{\Sigma} \qquad \text{(Eq. 5)}$$

Effect of Crosslinking Density of the Filler Network on the Accumulation and Localization of Damage during Fatigue Crack Propagation of DN Elastomers

The visualization and quantification of damage by sacrificial bond scission in fractured specimens is a novel tool to understand the role of the crosslinking density of the filler network on the crack growth rate of DN elastomers subject to cyclic loading. However, interpreting spatially resolved information on damage is challenging because of the complex relationship between the applied energy release rate $\mathcal{G}$ (or strain λ) and the resulting crack growth rate *dc/dN* and damage per unit area of crack propagation $\bar{\Sigma}$.

As illustrated in Fig. 4, the tougher and more extensible $EA_{0.2}EA$ suffers more damage than $EA_{0.5}EA$ when fractured under cyclic loading at the same applied energy release rate $\mathcal{G} \approx 1.0$ kJ.m^{-2}. The damage maps in Fig. 4A are rather homogeneous along the crack length *x* and specimen thickness *z*, with some inhomogeneous artifacts attributed to image stitching and optical vignetting (see details in the SI). This observation is consistent with the featureless side view of the fracture surface (see images for the plane *z* = 100 μm in Fig. 4B) and the monotonically decreasing *y*-profiles of damage from the crack surface ϕ_y (Fig. 4C). Interestingly, $EA_{0.2}EA$ exhibits a considerably higher *dc/dN* than $EA_{0.5}EA$ at the same $\mathcal{G} \approx 1.0$ kJ.m^{-2} (compare fatigue curves in Fig. 2C), meaning that less cycles *N* result in more damage $\bar{\Sigma}$ for the same unit area of crack growth.

Fig. 4 also illustrates changes in damage localization with the crosslinking density of the filler network. Although it is difficult to unambiguously define damage localization, we estimated the thickness of the surface layer over which the DN elastomers are damaged from the distance over which ϕ_y decreases to half its maximum value, $L_{1/2}$. $EA_{0.5}EA$ has a larger $L_{1/2}$ than $EA_{0.2}EA$ (compare *y*-profiles of ϕ_y in Fig. 4C), indicating that stiffening the filler network results in a more delocalized and gradual decrease of damage ahead of the crack tip during fatigue crack propagation (see schemes of damage zones Fig. 4D).

Thus, the crosslinking density of the filler network affects both the accumulation $\bar{\Sigma}$ and localization $L_{1/2}$ of damage ahead of the crack tip. We attribute this effect to differences in the large strain behavior between the two DN elastomers. Even though $EA_{0.2}EA$ and $EA_{0.5}EA$ require somewhat similar bulk strains to attain the same applied energy release rate $\mathcal{G}$ (see Table 2), the local strain of $EA_{0.2}EA$ ahead of the crack tip (*i.e.*, inside the damage zone) must be significantly larger than that of $EA_{0.5}EA$ because of its higher extensibility (we did not measure the strain at the crack tip, but we can infer the qualitative strain fields of Fig. 4D from images of crack blunting in Fig. S10). Large strains ahead of the crack tip increase the probability of damage by sacrificial bond scission, promote stress transfer to the matrix network, and favor crack growth. As such, $EA_{0.2}EA$ is more damaged than $EA_{0.5}EA$ per loading cycle, meaning that more Lake and Thomas monolayers of polymer chains break in the filler network of the more extensible DN elastomer upon crack growth. To better understand the role of bond scission on fatigue crack propagation, we also systematically quantified the damage of the two DN elastomers across a range of applied energy release rates $\mathcal{G}$.

Stable Damage Zone for Durability

Beyond the structure-property relationships of DN elastomers, the visualization and quantification of damage by sacrificial bond scission also serves to build a multi-scale picture of fatigue fracture. As illustrated in Fig. 5, the damage per unit area of crack growth $\bar{\Sigma}$ increases with the applied energy release rate $\mathcal{G}$ with a power law $\bar{\Sigma} \sim \mathcal{G}^{2.1}$. This scaling exponent is lower than that observed for the crack growth rate, $dc/dN \sim \mathcal{G}^{3.4}$ (Fig. 2C) and indicates that damaging DN elastomers results in a more significant increase in dc/dN. Interestingly, fracture under cyclic loading at high applied $\mathcal{G}$ requires less cycles N and results in more damage per unit area of crack growth $\bar{\Sigma}$. Thus, numerous cycles at low deformation are less damaging than few cycles at large deformation, or namely, more energy is dissipated by sacrificial bond scission when transitioning from cyclic to monotonic loading.

Details of the catastrophic failure under cyclic loading are also revealed by inspecting the post-mortem damage maps of the two coexisting regimes of crack growth at high applied $\mathcal{G}$ (see filled and empty squares in Fig. 2C and Fig. 5). DN elastomers are more damaged in the *slow* than in the *fast* crack growth regime (compare *fast* and *slow* damage maps of either $EA_{0.5}EA$ cycled at $\mathcal{G} \approx 2.1$ kJ.m^{-2} in Fig. 6A, or of $EA_{0.2}EA$ cycled at $\mathcal{G} \approx 0.8$ kJ.m^{-2} in Fig. S6), having maps with heterogeneities (*i.e.*, hotspots) that indicate damage accumulation at or near crack bifurcations (see representative images for the plane z = 100 μm in Fig. 6B). These damage heterogeneities are sometimes reflected in the *y*-profiles of ϕ_y, but sometimes lost in the *xz*-average (Eq. 1) due to insufficient damage accumulation in the crack bifurcations (compare *y*-profiles in Fig. 6C). Nonetheless, the *y*-profiles of ϕ_y can be used to estimate an average $\bar{\Sigma}$ and $L_{1/2}$ and better understand fatigue fracture (Table 3). Accumulation of damage over a large region ahead of many bifurcations is associated with a low dc/dN, whereas localization of damage over a small region ahead of few bifurcations is associated with a high dc/dN (see schemes of damage zones in Fig. 6D). This interplay between accumulation and localization of damage is also evidenced in the fracture surfaces (see SEM images in Fig. S11), which exhibit many bifurcation events in both regimes but are rougher when the crack grows slowly. As such, DN elastomers experience a fluctuating *local energy release rate* $\mathcal{G}_{local}$ ahead of the crack tip which depends on the bulk strain, but also on the mesoscopic bifurcation of the crack front and on the probability of sacrificial bond scission inside the damage zone. A fluctuating $\mathcal{G}_{local}$ is consistent with the discontinuous crack growth (Fig. 2B) and the catastrophic dc/dN observed at $\mathcal{G} \ll \mathcal{G}_c$ for $EA_{0.2}EA$ (Fig. 2C) during fatigue crack propagation.

A multi-scale picture of fatigue crack propagation results from damage quantification over a range of applied $\mathcal{G}$ and is based on two stages: formation of a damage zone and crack growth. This mechanism is similar to that postulated by Williams for glassy polymers like PMMA, where cyclic loading leads to a plastic zone prior to fracture (*27*). At low applied $\mathcal{G}$, the stress is primarily sustained by the filler network, there is random scission of sacrificial bonds ahead of the crack tip, and crack growth is controlled by the maximum extensibility of the matrix network. This matrix network is the same for both DN elastomers, and the more strain hardened elastomer, $EA_{0.5}EA$, has the lower probability of crack growth. At high applied $\mathcal{G}$, an important fraction of the stress is transferred from the filler to the matrix network (*29*), and sacrificial bond scission can suddenly localize in a zone of reduced $\bar{\Sigma}$ and localized $L_{1/2}$ damage that leads to *fast* crack growth. This transition is similar to that observed by Millereau *et. al.* at the yield point of multiple-network elastomers of lower volume fraction of filler network $\phi^{FN} \approx 0.03$, where damage by sacrificial bond scission localizes at the fronts of a necked region (*14*), and is more likely to occur in the elastomer with the lower yield stress, $EA_{0.2}EA$ (we could not measure the yield stress of DN elastomers because it is lower than the stress at break, but we know it is lower in $EA_{0.2}EA$ from Millereau *et. al.* (*14*) and Chen *et. al* (*30*)). As such, $EA_{0.5}EA$ has a more stable damage zone, a lower probability of crack growth, and a better fatigue resistance than $EA_{0.2}EA$.

Interestingly, a more stable damage zone also increases the probability of crack growth through a bifurcated pathway. Upon bifurcation of the crack front, the applied $\mathcal{G}$ decreases to $\mathcal{G}_{local}$ (*i.e.*, the strain field becomes more homogeneous), and damage delocalizes ahead of coexisting crack fronts. This delocalization enables significant damage accumulation prior to crack growth and leads to more dramatic differences in $\bar{\Sigma}$ and $L_{1/2}$ between the *slow* and *fast* crack growth regimes in the more fatigue resistant elastomer, $EA_{0.5}EA$ (Table 3). As a result, damage by sacrificial bond scission and bifurcations of the crack front reinforce each other (*i.e.*, integrate a positive feedback loop) to control the macroscopic crack growth rate *dc/dN* of DN elastomers. These mechanisms operate at distinct length scales and depend on the areal density of sacrificial bonds, as well as on the applied load.

Stiffening the filler network strain hardens the region ahead of the crack tip, decreases the probability of sacrificial bond scission, and delocalizes damage over a large region of coexisting bifurcations. This damage zone is more stable to cyclic loading but dissipates less energy. As such, fatigue resistant elastomers capable of sustaining many cycles at low loads are not necessarily optimum in terms of energy dissipation and toughness. We explore this issue by quantifying damage in DN elastomers fractured under monotonic loading.

Energy Dissipation for Toughness

To assess the ability of DN elastomers to dissipate energy, we monitored the crack length *c* of a pre-cracked pure-shear specimen subjected to monotonic loading at a fixed stretch rate, $\dot{\lambda}$, until fracture (see crack growth curves in Fig. 7B and Fig. S4, and videos of pure-shear fracture tests in Movies S3-S4). As illustrated in Fig. 7B, catastrophic *propagation* is preceded by a regime of slow crack growth that we refer to as *initiation*.

Like fracture under cyclic loading, the crosslinking density of the filler network has a significant effect on the accumulation and localization of damage during monotonic fracture. $EA_{0.5}EA$ exhibits more heterogeneous damage maps than $EA_{0.2}EA$ irrespective of whether the crack grows in the *initiation* or *propagation* regime (compare damage maps in Fig. 8A, roughness of fracture surfaces in Fig. S12, and fluorescent images for $z = 100\ \mu m$ in Fig. S13), indicating that it is more

prone to damage delocalization through bifurcation of the crack front. The *y*-profiles of ϕ_y also reveal that $EA_{0.5}EA$ accumulates $\bar{\Sigma}$ and delocalizes $L_{1/2}$ more damage than $EA_{0.2}EA$ during crack initiation, but not during crack propagation (see Fig. 8B, Fig. 8C and Table 4). This change in the damage zone is consistent with the trade-off between fatigue resistance and toughness, and in agreement with molecular models that describe the toughness of DN hydrogels and glassy polymers (*31*, *32*). DN elastomers capable of accumulating and delocalizing damage at $\mathcal{G} < \mathcal{G}_c$ should be more fatigue resistant, whereas those that dissipate more energy at $\mathcal{G} \approx \mathcal{G}_c$ should be tougher. Interestingly, the energy dissipated by sacrificial bond scission Γ_d can be estimated with Eq. 5 and is only ≈ 5% of the fracture energy $\mathcal{G}_c$, suggesting that other molecular processes such as polymer chain friction and stress transfer to the matrix network are important for toughening.

Quantification of damage by sacrificial bond scission serves to rationally engineer tough and fatigue resistant elastomers. Under monotonic loading, softening the filler network toughens DN elastomers because more energy is dissipated at the critical energy release rate $\mathcal{G}_c$, whereas stiffening the filler network improves the fatigue resistance of DN elastomers because the damage zone is more stable to cyclic loading at sub-critical energy release rates $\mathcal{G}$. To the best of our knowledge, this is the first clear demonstration of the role of network architecture on the damage zone, as well as on the trade-off between mechanical durability and fracture toughness.

Concluding Remarks

Soft and tough elastomers with a multiple-network architecture exhibit a trade-off between fatigue resistance and fracture toughness. While dissipating energy by sacrificial bond scission over large damage zones remains essential for resisting crack propagation at high loads, stabilizing the damage zone by mitigating the accumulation and localization of sacrificial bond scission events is critical for sustaining numerous cycles of low load. We have demonstrated that a stable damage zone is attained in DN elastomers by stiffening the filler network (*i.e.*, strain hardening the region ahead of the crack tip) to reduce the probability of sacrificial bond scission and promote bifurcation of the crack front. Given the similarity in composition, modulus, and bulk hysteresis of $EA_{0.2}EA$ and $EA_{0.5}EA$; this inversion in reinforcement when transitioning from monotonic to cyclic loading is noteworthy.

Cycling the fatigue resistant elastomer, $EA_{0.5}EA$, for 400,000 cycles at low applied energy release rates $\mathcal{G} \approx \mathcal{G}_0 \approx 550$ J.m^{-2} leads to negligible crack growth. This cyclic fatigue threshold is significantly higher than that of conventional elastomers and intrinsic to the multiple-network architecture. However, DN elastomers suffer from strain-dependent damage under cyclic loading, developing a zone of accumulated and delocalized damage at high applied energy release rates $\mathcal{G}$ which is prone to sudden localization and fast crack growth. This dependence of damage on the applied load serves as experimental evidence to refine current molecular models of fracture, like that of Lake and Thomas (*6*) and Olsen and co-workers (*33*), where the contribution of damage to the fracture energy results only from scission of stretched polymer chains in a damage zone of mesh-size.

DN elastomers tagged with mechanofluorescent probes provide novel insights on fatigue crack propagation. Upon polymer chain elongation until failure, these probes turn into fluorescent moieties of high quantum yield, stability to photobleaching, and ideal for quantifying cumulative damage by sacrificial bond scission in specimens that suffer negligible damage per unit time. As such, this combination of network design and damage quantification has enormous potential to understand fracture of soft materials under a range of complex loading configurations like multiaxial fatigue, cavitation, among others.

References

1. A. N. Gent, *Engineering with Rubber* (Hanser, ed. 3rd, 2012; http://www.sciencedirect.com/science/article/pii/B9783446427648500181).
2. G. J. Lake, Fatigue and Fracture of Elastomers. *Rubber Chem. Technol.* **68**, 435–460 (1995).
3. W. V Mars, A. Fatemi, Factors that Affect the Fatigue Life of Rubber: A Literature Survey. *Rubber Chem. Technol.* **77**, 391–412 (2004).
4. A. N. Gent, P. B. Lindley, A. G. Thomas, Cut growth and fatigue of rubbers. I. The relationship between cut growth and fatigue. *J. Appl. Polym. Sci.* **8**, 455–466 (1964).
5. G. J. Lake, P. B. Lindley, Cut growth and fatigue of rubbers. II. Experiments on a noncrystallizing rubber. *J. Appl. Polym. Sci.* **8**, 707–721 (1964).
6. G. J. Lake, P. B. Lindley, The mechanical fatigue limit for rubber. *J. Appl. Polym. Sci.* **9**, 1233–1251 (1965).
7. S. Mzabi, D. Berghezan, S. Roux, F. Hild, C. Creton, A critical local energy release rate criterion for fatigue fracture of elastomers. *J. Polym. Sci. Part B Polym. Phys.* **49**, 1518–1524 (2011).
8. C. Li, H. Yang, Z. Suo, J. Tang, Fatigue-Resistant elastomers. *J. Mech. Phys. Solids*. **134**, 103751 (2020).
9. J. Tang, J. Li, J. J. Vlassak, Z. Suo, Fatigue fracture of hydrogels. *Extrem. Mech. Lett.* **10**, 24–31 (2017).
10. R. Bai, Q. Yang, J. Tang, X. P. Morelle, J. Vlassak, Z. Suo, Fatigue fracture of tough hydrogels. *Extrem. Mech. Lett.* **15**, 91–96 (2017).
11. W. Zhang, X. Liu, J. Wang, J. Tang, J. Hu, T. Lu, Z. Suo, Fatigue of double-network hydrogels. *Eng. Fract. Mech.* **187**, 74–93 (2018).
12. R. Bai, J. Yang, Z. Suo, Fatigue of hydrogels. *Eur. J. Mech. - A/Solids*. **74**, 337–370 (2019).
13. J.-Y. Sun, X. Zhao, W. R. K. Illeperuma, O. Chaudhuri, K. H. Oh, D. J. Mooney, J. J. Vlassak, Z. Suo, Highly stretchable and tough hydrogels. *Nature*. **489**, 133–136 (2012).
14. P. Millereau, E. Ducrot, J. M. Clough, M. E. Wiseman, H. R. Brown, R. P. Sijbesma, C. Creton, Mechanics of elastomeric molecular composites. *Proc. Natl. Acad. Sci.* **115**, 9110–9115 (2018).
15. Y. Tanaka, R. Kuwabara, Y.-H. Na, T. Kurokawa, J. P. Gong, Y. Osada, Determination of Fracture Energy of High Strength Double Network Hydrogels. *J. Phys. Chem. B.* **109**, 11559–11562 (2005).
16. E. Ducrot, Y. Chen, M. Bulters, R. P. Sijbesma, C. Creton, Toughening Elastomers with Sacrificial Bonds and Watching Them Break. *Science (80-.).* **344**, 186–189 (2014).
17. R. Göstl, R. P. Sijbesma, π-extended anthracenes as sensitive probes for mechanical stress. *Chem. Sci.* **7**, 370–375 (2016).
18. M. Stratigaki, C. Baumann, L. C. A. van Breemen, J. P. A. Heuts, R. P. Sijbesma, R. Göstl, Fractography of poly(N -isopropylacrylamide) hydrogel networks crosslinked with mechanofluorophores using confocal laser scanning microscopy. *Polym. Chem.* **11**, 358–366 (2020).
19. J. Slootman, V. Waltz, C. J. Yeh, C. Baumann, R. Göstl, J. Comtet, C. Creton, Quantifying Rate- and Temperature-Dependent Molecular Damage in Elastomer Fracture. *Phys. Rev. X.* **10**, 041045 (2020).
20. R. S. Rivlin, A. G. Thomas, in *Collected Papers of R.S. Rivlin* (Springer New York, New York, NY, 1997; http://link.springer.com/10.1007/978-1-4612-2416-7_180), vol. X, pp. 2615–2642.

21. R. Long, C.-Y. Hui, Fracture toughness of hydrogels: measurement and interpretation. *Soft Matter*. **12**, 8069–8086 (2016).
22. Y. N. Lenets', Near-threshold fatigue-crack growth: State of the problem and some anomalies. *Mater. Sci.* **30**, 301–315 (1995).
23. G. J. Lake, A. G. Thomas, The Strength of Highly Elastic Materials. *Proc. R. Soc. A Math. Phys. Eng. Sci.* **300**, 108–119 (1967).
24. A. Ahagon, A. N. Gent, Threshold fracture energies for elastomers. *J. Polym. Sci. Polym. Phys. Ed.* **13**, 1903–1911 (1975).
25. A. N. Gent, R. H. Tobias, Threshold tear strength of elastomers. *J. Polym. Sci. Polym. Phys. Ed.* **20**, 2051–2058 (1982).
26. J. P. Gong, Y. Katsuyama, T. Kurokawa, Y. Osada, Double-network hydrogels with extremely high mechanical strength. *Adv. Mater.* **15**, 1155–1158 (2003).
27. J. G. Williams, A model of fatigue crack growth in polymers. *J. Mater. Sci.* **12**, 2525–2533 (1977).
28. S. Wang, S. Panyukov, M. Rubinstein, S. L. Craig, Quantitative Adjustment to the Molecular Energy Parameter in the Lake–Thomas Theory of Polymer Fracture Energy. *Macromolecules*. **52**, 2772–2777 (2019).
29. Y. Chen, C. J. Yeh, Y. Qi, R. Long, C. Creton, From force-responsive molecules to quantifying and mapping stresses in soft materials. *Sci. Adv.* **6**, eaaz5093 (2020).
30. Y. Chen, C. J. Yeh, Q. Guo, Y. Qi, R. Long, C. Creton, Fast reversible isomerization of merocyanine as a tool to quantify stress history in elastomers. *Chem. Sci.* (2021), doi:10.1039/D0SC06157C.
31. H. R. Brown, A molecular interpretation of the toughness of glassy polymers. *Macromolecules*. **24**, 2752–2756 (1991).
32. H. R. Brown, A Model of the Fracture of Double Network Gels. *Macromolecules*. **40**, 3815–3818 (2007).
33. A. Arora, T.-S. Lin, H. K. Beech, H. Mochigase, R. Wang, B. D. Olsen, Fracture of Polymer Networks Containing Topological Defects. *Macromolecules*. **53**, 7346–7355 (2020).

Acknowledgments: SEM images were collected by Guillaume Votte. **Funding:** This work was supported by the European Research Council (ERC) under the European Union's Horizon 2020 Research and Innovation Program (Grant Agreement N° 695351 – CHEMECH). X.P.M. was financially supported by the WBI world excellence post-doctoral fellowship. **Author contributions:** Research was designed by G.E.S., X.P.M., and C.C. Synthesis was conducted by G.E.S. Specimens were mechanically tested by G.E.S., and X.P.M. Damage was visualized and quantified by G.E.S., J.C., and C.J.Y. The manuscript was written by G.E.S., and critically revised by all authors. All authors have given final approval to the final version of the manuscript. **Competing interests:** Authors declare no competing interests. **Data and materials availability:** All data is available in the main text and supplementary materials. Additional information may be requested from the authors.

Figures and Tables

Table 1. Composition and mechanical properties of DN elastomers. Presented are the volume fraction ϕ^{FN}, pre-stretch λ_0, and maximum extensibility λ_m^{FN} of the filler network; as well as the Young's modulus E, strain at break λ_{break}, toughness $\mathcal{G}_c$, and areal density of sacrificial polymer chains Σ_0 of the double-networks.

	ϕ^{FN}	λ_0	λ_m^{FN}	E (MPa)	λ_{break}	$\mathcal{G}_c$ (kJ.m^{-2})	Σ_0 (chains.m^{-2})
$EA_{0.2}EA$	0.19	1.74	6.70	0.98	3.51	2.80	6.0 x 10^{16}
$EA_{0.5}EA$	0.22	1.67	4.89	1.05	2.74	1.97	9.2 x 10^{16}

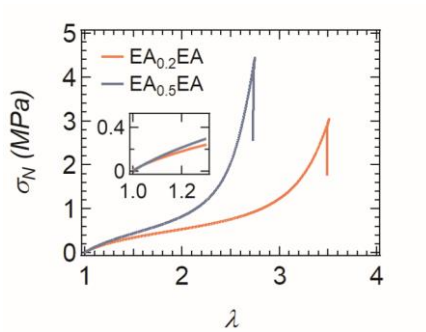

Fig. 1. Uniaxial deformation of DN elastomers. $EA_{0.2}EA$ and $EA_{0.5}EA$ have a similar modulus (inset) but a different onset of strain hardening and strain at break.

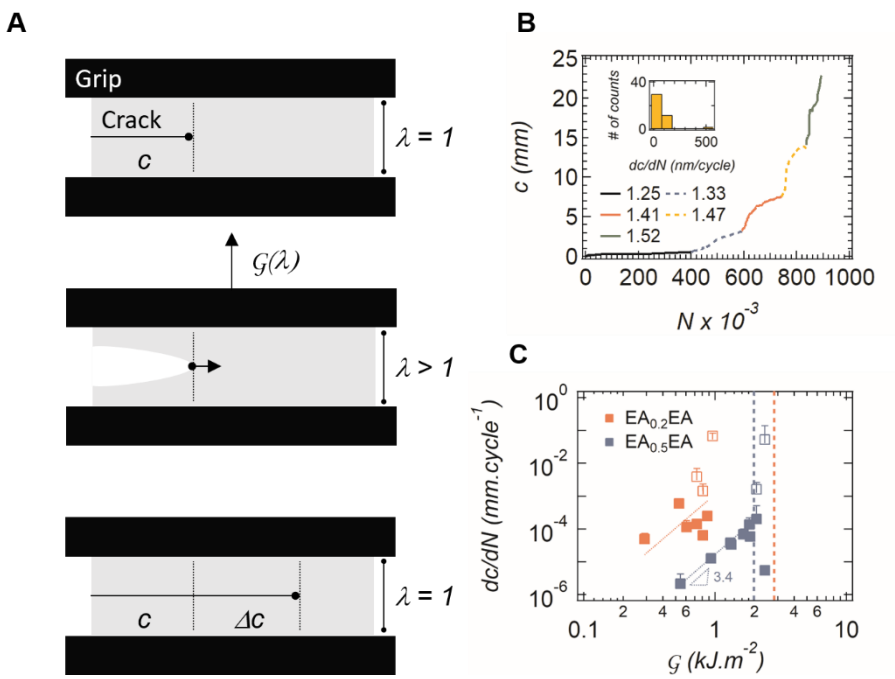

Fig. 2. Fatigue crack propagation of DN elastomers. (**A**) Schematic of a pure shear fatigue fracture test. The pure shear geometry is ideal for studying fracture because the applied energy release rate $\mathcal{G}(\lambda)$ is independent of crack length c (20, 21). (**B**) Crack growth of $EA_{0.5}EA$ is discontinuous and dependent on the applied stretch λ and energy release rate $\mathcal{G}(\lambda)$. (Inset) Representative distribution of crack growth rates dc/dN for $\lambda = 1.47$ or $\mathcal{G}(\lambda) =$ 1642 J.m^{-2}. A similar fracture behavior is observed for $EA_{0.2}EA$ (Fig. S5A). (**C**) Fatigue crack propagation of $EA_{0.2}EA$ and $EA_{0.5}EA$. $EA_{0.5}EA$ is more fatigue resistant than $EA_{0.2}EA$ despite its lower toughness $\mathcal{G}_c$ (dashed vertical lines). Open (☐) and closed (■)

symbols respectively correspond to *fast* and *slow* crack growth regimes. Error bars represent 95% confidence intervals.

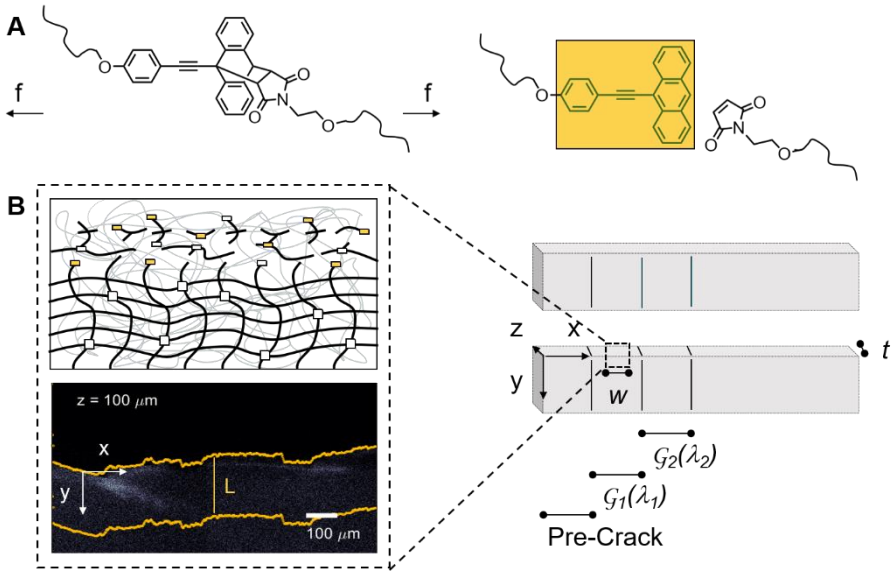

Fig. 3. Post-mortem mapping of damage by sacrificial bond scission. (**A**) Mechanophores based on π-extended anthracene-maleimide adducts yield π-extended anthracene moieties upon force-induced cycloreversion. (**B**) Fluorescent microscopy in a fractured specimen reveals high internal damage near the crack surface and around crack bifurcations. Damage by polymer chain scission is quantified over a distance L = 300 μm from the crack surface. Energy release rates $\mathcal{G}_i(\lambda_i)$ were applied in a subsequent and stepwise fashion to optimize the use of tagged and probe-expensive pure-shear specimens.

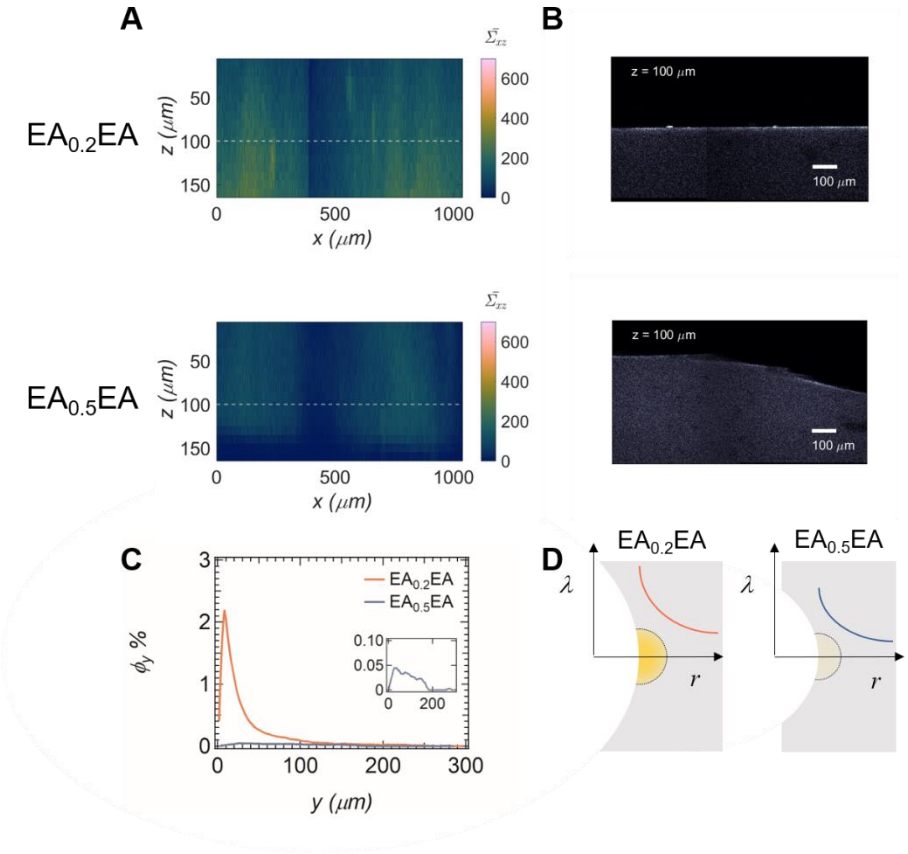

Fig. 4. Damage of DN elastomers fractured under cyclic loading at $\mathcal{G} \approx 1.0$ kJ.m^{-2}. (**A**) Spatial maps of local damage per unit area of crack propagation, $\overline{\Sigma_{xz}}$, reveal that $EA_{0.2}EA$ is more damaged than $EA_{0.5}EA$. (**B**) Representative images at z = 100 μm (white dashed line in Fig. 4A) illustrate that featureless fracture surfaces are associated with homogeneous damage maps along the crack length. (**C**) Profiles of sacrificial bond scission ϕ_y reveal that $EA_{0.2}EA$ has a more concentrated and localized damage zone than $EA_{0.5}EA$. (Inset) Enlarged profile of sacrificial bond scission ϕ_y of $EA_{0.5}EA$ (**D**) Schemes of damage zones of DN elastomers undergoing fatigue crack propagation. $EA_{0.5}EA$ has reduced and delocalized damage ahead of the crack tip and, as such, can sustain many cycles of low deformation prior to crack growth.

Table 2. Loading conditions and damage properties of DN elastomers fractured under cyclic loading at $\mathcal{G} \approx 1.0$ kJ.m^{-2}. Presented are the applied stretch λ, energy release rate $\mathcal{G}$, crack growth rate *dc/dN*, overall damage per unit area of crack propagation $\bar{\Sigma}$, and the damage penetration length $L_{1/2}$.

	λ	$\mathcal{G}$ (J.m^{-2})	$dc/dN \times 10^5$ (mm.cycle^{-1})	$\bar{\Sigma}$	$L_{1/2}$ (μm)
$EA_{0.2}EA$	1.57	956	6800	94	23
$EA_{0.5}EA$	1.33	932	1.27	12	128

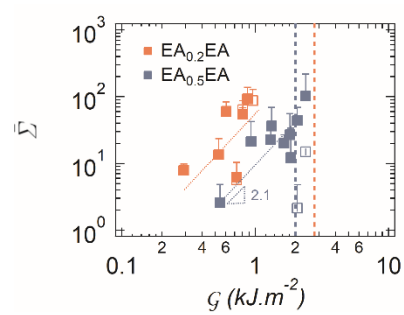

Fig. 5. Damage of DN elastomers fractured under cyclic loading over a range of $\mathcal{G}$. $EA_{0.2}EA$ is more damaged than $EA_{0.5}EA$ over the entire range of applied energy release rates $\mathcal{G}(\lambda)$. In addition, both $EA_{0.2}EA$ and $EA_{0.5}EA$ are more damaged at high energy release rates $\mathcal{G}$ even though less cycles N are required to attain the same unit area of crack growth. Open (☐) and closed (■) symbols respectively correspond to *fast* and *slow* crack growth regimes. Dashed vertical lines indicate the fracture toughness $\mathcal{G}_c$. Error bars represent 95% confidence intervals.

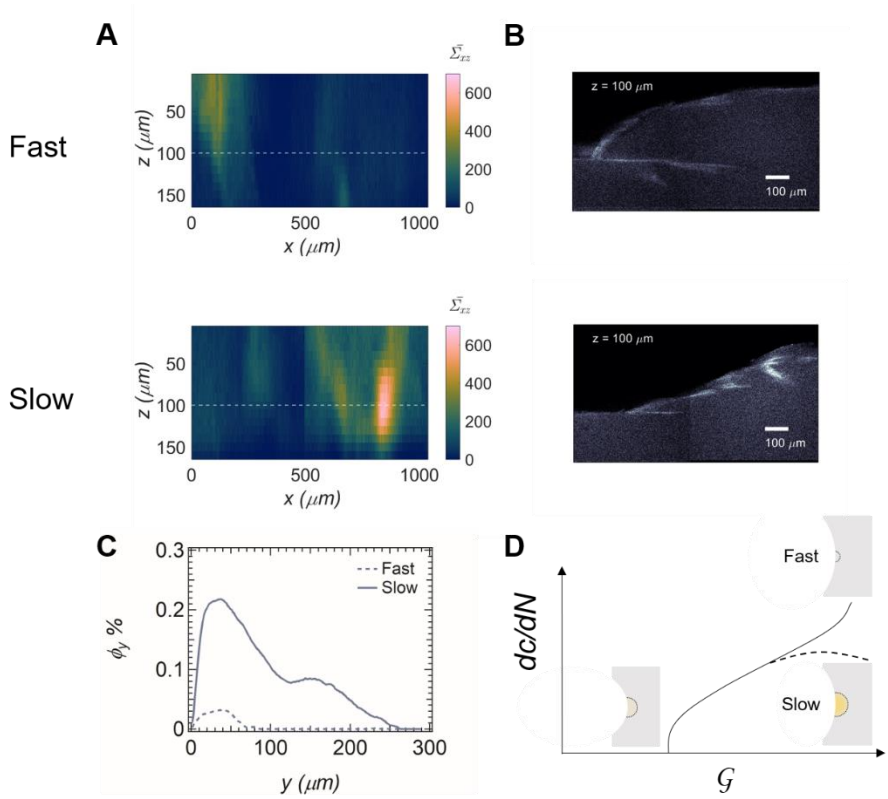

Fig. 6. Damage of $EA_{0.5}EA$ fractured under cyclic loading at $\mathcal{G} \approx 2.1$ kJ.m^{-2}. (**A**) Spatial maps of local damage per unit area of crack propagation $\overline{\Sigma_{xz}}$ reveal that $EA_{0.5}EA$ is more damaged in the *slow* than in the *fast* crack growth regime. (**B**) Representative images at *z* = 100 μm (white dashed line in Fig. 6A) illustrate that crack bifurcations are associated with hotspots in damage maps. (**C**) Profiles of sacrificial bond scission ϕ_y reveal that $EA_{0.5}EA$ undergoes catastrophic crack propagation due to sudden localization of damage ahead of the crack tip. (**D**) Schematics of the damage zone of $EA_{0.5}EA$ in the *slow* and *fast* crack growth regimes. Fast crack growth is associated with a highly localized and reduced damage ahead of the crack tip.

Table 3. Loading conditions and damage properties of DN elastomers fractured under cyclic loading at high applied energy release rates $\mathcal{G}$. Presented are the applied stretch λ, energy release rate $\mathcal{G}$, crack growth rate *dc/dN*, overall damage per unit area of crack propagation $\bar{\Sigma}$, and the damage penetration length $L_{1/2}$.

	λ	$\mathcal{G}$ (J.m^{-2})	*Regime*	*dc/dN x 10^5 (mm.cycle^{-1})*	$\bar{\Sigma}$	$L_{1/2}$ (μm)
$EA_{0.2}EA$	1.49	808	Fast	144	40	54
			Slow	6.40	62	70
$EA_{0.5}EA$	1.62	2069	Fast	161	4	60
			Slow	20.0	62	101

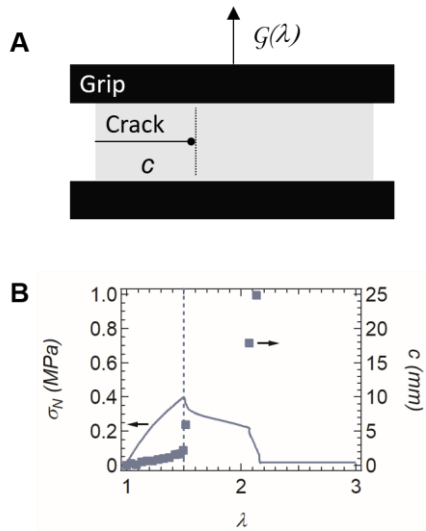

Fig. 7. Fracture of DN elastomers under monotonic loading. (**A**) Schematics of a pure-shear fracture test. (**B**) Crack growth and loading curve of $EA_{0.5}EA$. The crack growth transitions from the *initiation* to the *propagation* regime at the critical stretch λ_c (dashed vertical line).

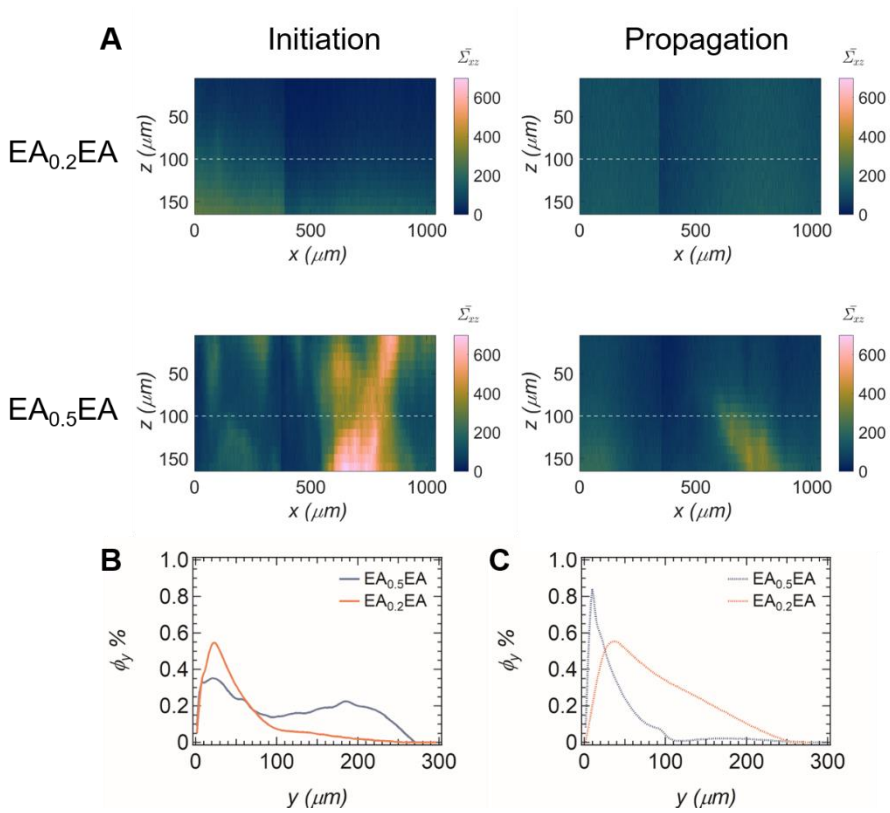

Fig. 8. Damage of DN elastomers fractured under monotonic loading. (**A**) Spatial maps of $\overline{\Sigma_{xz}}$ reveal that $EA_{0.5}EA$ exhibits a more heterogeneous damage than $EA_{0.2}EA$ in the *initiation* and *propagation* regimes. Profiles of ϕ_y during crack (**B**) initiation and (**C**) propagation illustrate that the length scale over which bonds are broken depends on whether the energy supplied during loading is above or below $\mathcal{G}_c$.

Table 4. Damage properties of DN elastomers fractured under monotonic loading. Presented are the overall damage per unit area of crack propagation $\bar{\Sigma}$, and the penetration length $L_{1/2}$.

	Regime	$\bar{\Sigma}$	$L_{1/2}$ (μm)
$EA_{0.2}EA$	Initiation	55	58
	Propagation	107	131
$EA_{0.5}EA$	Initiation	123	75
	Propagation	77	35